Proceedings of the Twenty-seventh (2017) International Ocean and Polar Engineering Conference **www.isope.org**
San Francisco, CA, USA, June 25-30, 2017

ISBN 978-1-880653-97-5; ISSN 1098-6189

Computation of Wave Drift Forces and Motions of DTC Ship in Oblique Waves

Cong Liu[1], *Jianhua Wang*[1], *Decheng Wan*[1]*, *Xinguo Yu*[2]
[1] Collaborative Innovation Center for Advanced Ship and Deep-Sea Exploration, State Key Laboratory of Ocean Engineering, School of Naval Architecture, Ocean and Civil Engineering, Shanghai Jiao Tong University, Shanghai, China
[2] China Ship Development and Design Center, Shanghai Branch, China
*Corresponding author

ABSTRACT

To assess ship maneuverability in waves, computations of a ship with heave, roll and pitch motions in oblique wave are presented. The wave drift forces, heave and pitch motions are investigated numerically. The computations are based on volume of fluid (VOF) and overset mesh methods, discretized by finite volume method (FVM). An open source library, wave2Foam, is used to generate desired wave conditions. Seven wave conditions with a wide range of incident angle are considered. The wavelength is in the range of short waves and the results show strong nonlinear features, especially for beam wave and following waves, where the phenomenon of wave breaking on port side and stern is observed. The comparison of wave drift forces between the present computational results and measurements shows good agreement.

KEY WORDS: Wave drift forces; naoe-FOAM-SJTU solver; overset grid; oblique wave; DTC ship model

INTRODUCTION

The background of the presented research is the implementation of the Energy Efficiency Design Index (EEDI), by the IMO in January 2013 and the associated requirement for each new-built vessel to meet reference lines for vessel emissions. To meet the EEDI requirements, some ship designers/builders choose to lower the installed power and ship's speed instead of putting effort to optimize ship's speed-powering performance. It leads to raise concerns regarding the sufficiency of propulsion power and steering devices to maintain maneuverability of ships in adverse conditions. It is evident that when a ship is operating in adverse weather conditions, wave drift forces and moments will act on ship and change its course. Therefore, it is necessary to develop suitable tools to effectively evaluate wave drift forces and moments and to enable people assess ship maneuverability in waves.

To address these issues, extensive experimental and numerical investigations were performed within the European funded Project SHOPERA. In this project, one of the tested ship selected for benchmark and validation was a post-Panamax 14000 TEU containership, the Duisburg Test Case (DTC). To gain the drift forces of DTC, systematical test cases consisting of different drift angles were conducted in the European maritime experimental research institutes MARINTEK. Basing on their experimental data, we use CFD solver, naoe-FOAM-SJTU (Shen and Wan, 2011; Shen et al., 2012; Shen and Wan, 2012; Cao et al., 2013), to perform simulations on DTC and calculate the drift forces in the expectation of obtaining some details of DTC's hydrodynamic characteristics.

There are many previous studies focusing on wave drift forces, most of which are using the potential theory. Grue and Palm (1993) discussed the effect of the steady second-order velocities on the drift forces and moments acting on marine structure in waves and a (small) current. Following that, Hermans (1999) presented numerical results for two classes of tankers, namely for a VLCC and a LNG-carrier, and a semi-submersible and compared with experimental data obtained at the Maritime Research Institute in the Netherlands (MARIN). Tanizawa et al. (2000) applied a linear and a fully nonlinear numerical wave tanks (NWTs) to study wave drift force acts on a two-dimensional Lewis form body in finite depth wave flume.

However, the conventional potential methods still have limitations when handling strong nonlinear problems. Owing to the rapid development of computer power, computational fluid dynamics (CFD) has experienced unprecedented developments in recent decades. Since reliable multiphase models and turbulence models are developed, CFD can handle more nonlinear problems and obtain more accurate results.

In the view of above, there are plenty of studies focused on ship motions in waves by using CFD methods. For example, Orihara and Miyata (2003) solved ship motions under regular head wave conditions and evaluated the added resistance of an SR-108 container ship in waves using a CFD simulation method called WISDAM-X. The Reynolds-averaged Navier–Stokes (RANS) equation was solved using the finite volume method with an overlapping grid system. Shen et al. (2012) conducted numerical simulations of DTMB model 5512 in regular head waves by an OpenFOAM based solver naoe-FOAM-SJTU. Sadat-Hosseini et al. (2013) presented added resistance results for KVLCC2 through both experimental and numerical methods. Yang and Kim (2015) predicted the added resistance of KVLCC2 in waves. In that study, ship body was

represented by a signed distance function. More recently, in the work of Moctar (2016), second order forces and moments for DTC were measured in model tests and computed by solving the RANS equations.

In this paper, an incompressible method with two-phase interface is applied to simulate viscous flow around a ship in regular waves. Seven wave heading angles were considered. The ship speed is zero in these simulations, so laminar model is used to calculate the viscous forces instead turbulence model since the Reynold number is quite small. Predictions of heave, pitch and roll motions and wave drift forces are considered in this case. The predicted wave drift forces are compared with the experimental data. The coupled pressure and velocity fields are solved by merged PISO-SIMPLE (PIMPLE) algorithm. The water-air interface is captured by a VOF method with a compression technique (MULES). A six-degree-of-freedom (6DoF) module coupled with overset grid technique (Shen et al. 2015) is utilized to predict the motions of ship. Additionally, several built-in numerical schemes in OpenFOAM are used in solving the partial differential equation. The convection terms are discretized by a second-order total variation diminishing (TVD) limited linear scheme, and the diffusion terms are approximated by a second-order central difference scheme. Van Leer scheme is applied for VOF equation discretization and a second-order backward method is applied for temporal discretization.

This paper is organized as follows: In the first section, a brief introduction of the numerical methods is given. The geometry and setup of the computational cases are following. Next, the computational results and the comparison with experimental data are discussed. Finally, a summary of the paper is presented.

NUMERICAL METHODS

Governing Equations

The incompressible Navier-Stokes equations are the governing equations, which can be written as:

$$\nabla \cdot \mathbf{U} = \mathbf{0} \tag{1}$$

$$\frac{\partial \rho \mathbf{U}}{\partial t} + \nabla \cdot \left(\rho\left(\mathbf{U} - \mathbf{U_g}\right)\mathbf{U}\right) = -\nabla p_d - \mathbf{g} \cdot \mathbf{x} \nabla \rho + \nabla \cdot (\mu \nabla \mathbf{U}) \tag{2}$$

where U is fluid velocity field and $\mathbf{U}_g$ is the grid velocity; $p_d = p - \rho \mathbf{g} \cdot \mathbf{x}$ is the dynamic pressure, obtained by subtracting the hydrostatic component from the total pressure; ρ is the mixture density; $\mathbf{g}$ is the gravity acceleration; μ is dynamic viscosity.

VOF Method

The Volume of Fluid (VOF) method with artificial compression is used to capture the air/water interface. Details of the VOF solution procedure as implemented in OpenFOAM are described in Rusche (2002), and only a brief explanation is presented here. A VOF method with bounded compression technique is applied to capture free surface interface. The transport equation is expressed as

$$\frac{\partial \alpha}{\partial t} + \nabla \cdot \left(\rho\left(\mathbf{U} - \mathbf{U_g}\right)\alpha\right) + \nabla \cdot (\mathbf{U}_r(1-\alpha)\alpha) = 0 \tag{3}$$

where α is volume of fraction, indicating the relative proportion of fluid in each cell and its value is always between zero and one:

$$\begin{cases} \alpha = 0 & \text{air} \\ \alpha = 1 & \text{water} \\ 0 < \alpha < 1 & \text{interface} \end{cases} \tag{4}$$

In Eq. (3), $\mathbf{U}_r$ is the velocity field used to compress the interface and it takes effect only on the surface interface due to the term $(1-\alpha)\alpha$. The expression of this term can be found in Berberović et al. (2009).

Overset Grid Technique

Overset grid is a grid system composed of multiple blocks of overlapping structured or unstructured grids. In a full overset grid system, a complex geometry is decomposed into a system of geometrically simple overlapping grids. Boundary information is exchanged between these grids via interpolation of the fluid variables. Through this way overset grid method removes the restrictions of the mesh topology among different objects and allows grids move independently within the computational domain, and can be used to handle with large amplitude motion in the field of ship and ocean engineering. The most critical technique in the overset is the accomplishment of information exchange between grids. Based on the numerical methods from OpenFOAM including the cell-centered scheme and unstructured grids, SUGGAR++ is utilized to generate the domain connectivity information (DCI) for the overset grid interpolation in our solver naoe-FOAM-SJTU. Through this way, the solver can handle with arbitrary motion in the simulation. For example, Wang et al. (2016 a) used our solver to simulate ship self-propulsion with moving propellers and rudders. Furthermore, Wang et al. (2016 b) carried out turning circle simulation by our solver. In those study, the moving rudders and rotating propellers were handled by the dynamic overset grid method. More details about overset technique can be found in Shen et al. (2015).

Wave Generation

In order to implement the wave generation and absorption in computational domain, the open source library waves2Foam (Jacobsen et al. 2012) is imposed in our solver. In the work of Jacobsen et al. (2012), a technology called relaxation zones are implemented to avoid wave reflection between the boundaries. The relaxation zone achieves the functionality of both wave generation and absorption in a uniform way.

GEOMETRY AND CONDITIONS

The model chosen to calculate is Duisburg Test Case(DTC) and the comprehensive experiments data have been obtained by MARINTEK. The arrangement of this experiment can be find in Springer et al. (2016). DTC is a generic post-Panamax 14000 TEU containership developed at the Institute of Ship Technology, Ocean Engineering and Transport Systems (ISMT) of the University of Duisburg-Essen. Its lines and other characteristics are shown in Fig. 1, and its principal particulars are listed in Table 1 as model-scale values. Here L_{pp} is length between perpendiculars, B is molded breadth, CB is block coefficient, Δ is displacement, S_w is wetted hull surface without appendages, LCG is longitudinal distance of the center of gravity from the aft perpendicular, VCG is vertical distance of the center of gravity from the base line, GM_T is transverse metacentric height, and r_{xx}, r_{yy}, r_{zz}, are, longitudinal, transverse and vertical gyradius about the center of gravity, respectively. DTC design features a twisted rudder with Costa bulb and a NACA 0018 base profile (see Fig. 1, bottom).

On each sides of the vessel, a segmented bilge keel is placed symmetrically around the mid-ship section, but the keels are not considered in this study. the reason of this simplification is that the wave force impacting on the keel can be quite limited due to its small wet area.

The computations are conducted at a scale of 1:63.65.

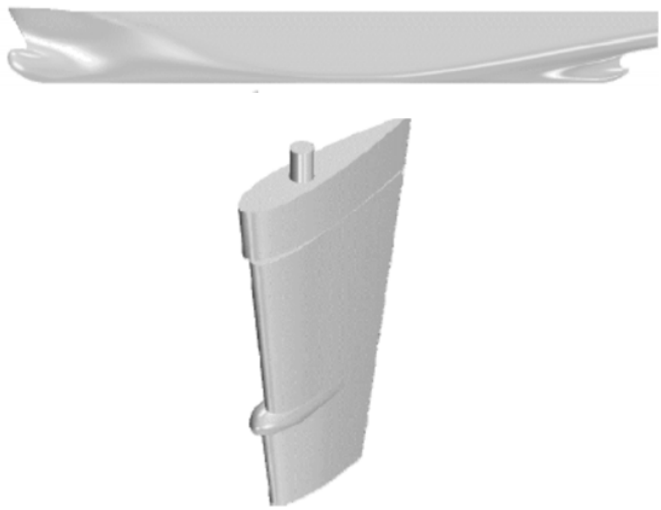

Fig. 1 View of Duisburg Test Case hull(top), rudder (bottom)

Table 1: Principal particulars of the DTC
(scale factor = 1:63.65)

Main particular	Value
λ	1:63.65
L_{pp}	5.57 m
B	0.80 m
T	0.23 m
CB	0.661
Δ	672.7 kg
S_w	5.438 m^2
LCG	2.74 m
VCG	0.39 m
GM_T	0.08 m
r_{xx}	0.31 m
r_{yy}	1.37 m
r_{zz}	1.37 m

This study focuses on the drift forces in different heading angle, therefore only one wave height and period is chosen, while the wave angle changes every 30°. Table 2 lists wave height, wave period, and wave heading angles for these simulations at zero knots. (Heading angle 0° refers to head waves.). All parameters are given in model scale. The setup confines the hull's surge, sway, and yaw motions and leaves it free to heave, roll, and pitch.

Table2 Cases conditions

Case no	Wave Height	Wave Period	Wave Angle
1	0.157m	1.128s	0
2	-	-	30
3	-	-	60
4	-	-	90
5	-	-	120
6	-	-	150
7	-	-	180

There are two grids for mesh region. One is called background grid and another one is hull grid which follows the motions of hull. The design of the overset grid system for the DTC is shown in Fig. 2. The hull grid resolves the near flow around the ship and the background grid accommodates the far-field boundary conditions and is refined at the free-surface. The computational domain extends $-1.0L_{pp} < x < 3.0L_{pp}$, $-1.5L_{pp} < y < 1.5L_{pp}$ and $-2.0L_{pp} < z < 1.0L_{pp}$. The grids interpolated by Suggar++ are illustrated in Fig. 3. Local refinements are applied at free surface and the region around the ship hull and the rudder. The two grids used in this paper are separately generated by SnappyHexMesh, an automatic mesh-generation utility provided by OpenFOAM. This utility generates mesh on an original cartesian background mesh, splitting hexahedral cells into split-hex cells. The view of computational mesh can be find in Fig.4. The sizes of these grids are listed in Table3. As the table showing, about 2 millions of cells are used in background grid. Majority of these cells distribute around the free-surface to make sure that the wave pattern does not decay before arriving to the hull.

To generate proper wave environment, the relaxation zone technique is used (Fig.5). Four relaxation zones are set up to avoid reflection of waves from outlet boundaries and further to avoid waves reflected internally in the computational domain to interfere with the wave maker boundaries. As illustrated in the Fig. 5, for head waves, the zones on the underside and the left are used to make oblique waves and the other two are used to absorb waves. Additional, for following waves, the position of wave generation zone on the left and wave absorption zone on the right are exchanged to generate following waves.

All computations were performed with 40 processors, one of which was assigned to Suggar++ for DCI computation. The time step is $\Delta t = 1 \times 10^{-3}$ s for heading angles less than or equal to 90 degrees, and $\Delta t = 5 \times 10^{-4}$ s for heading angles greater than 90 degrees. That makes sure the interface Courant Number less than 1, which is critical to keep cases convergent and simulations robust. The total clock time per time step is about 14s. It is quite effective comparing with deforming mesh technology which spends 21s per step. For the deforming mesh, it costs plenty times to calculate the mesh motion in each time step.

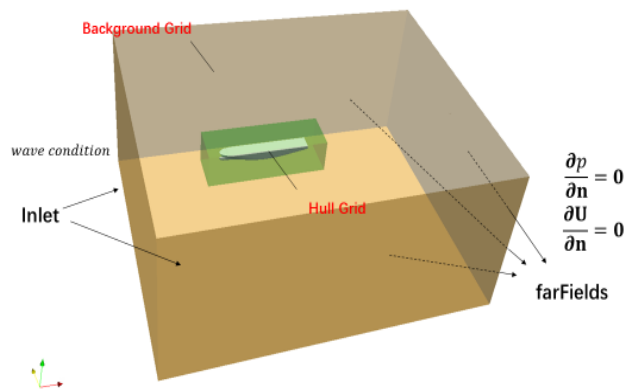

Fig. 2 Design of the overset grid system for DTC

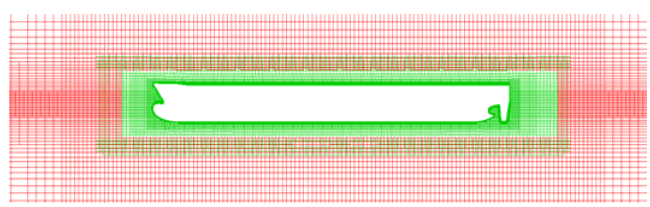

Fig. 3 Mesh views for vertical plane at y=0 (red for background mesh and green for hull mesh)

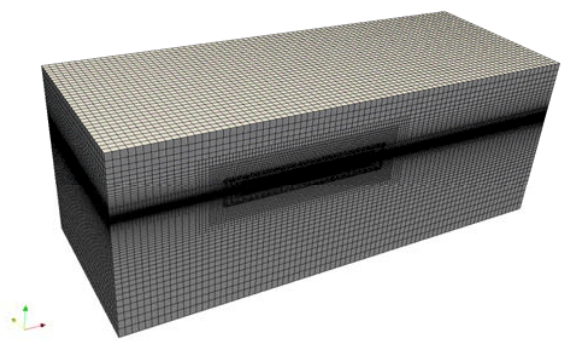

(a) Global Mesh (split along central fore-and-aft vertical plane)

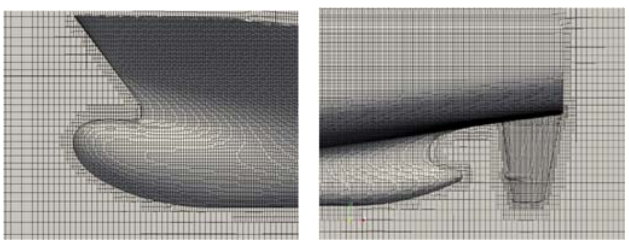

(b) Local Mesh (Bow) (c) Local Mesh (Stern)

Fig. 4 Computational mesh

Table 3 Grid sizes for DTC wave drift forces computations.

	Hull	Background	Total
Cells number	1,461919	2,226,624	3,688,543

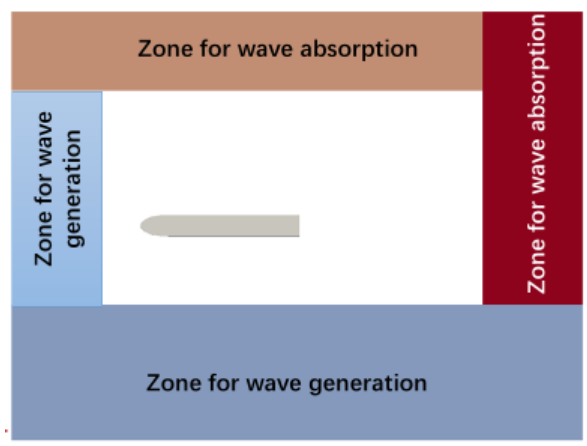

Fig. 5 Top-down view on a computational domain with wave generation zone

RESULTS

Wave Drift Forces

Fig.6 shows the results of dimensionless coefficients of longitudinal drift forces, lateral drift forces and yaw drift moments in the range of 0-180 degree heading angles. The definition of the coefficients are:

$$C_{fx} = \frac{\overline{F_x}}{\rho \cdot g \cdot \frac{B^2}{L_{pp}} \left(H/_2\right)^2} \quad (5)$$

$$C_{fy} = \frac{\overline{F_y}}{\rho \cdot g \cdot \frac{B^2}{L_{pp}} \left(H/_2\right)^2} \quad (6)$$

$$C_{fzm} = \frac{\overline{M_z}}{\rho \cdot g \cdot B^2 \cdot \left(H/_2\right)^2} \quad (7)$$

Where $\overline{F_x}$, $\overline{F_y}$ and $\overline{M_z}$ are the time average of longitudinal forces ,lateral forces and yaw moments; L_{pp} and B are length between perpendiculars and molded breadth respectively; H is the wave height. Results are compared with experimental measurements from MARINTEK available from the SHOPERA Benchmark Workshop (Potthoff et al.2016).

In general, an overall agreement is achieved. Computational results of the C_{fx} have the same trend with the experimental data .Both EFD and numerical results of C_{fx} show that the absolute values of C_{fx} are greater in the following wave condition comparing with the head wave condition. For example, comparing the C_{fx} results between 0° and 180°, it is obvious that the C_{fx} of 180° is twice bigger than that of 0°. Similarly, The C_{fx} of 150° is around 1.5 times as large as that of 30°. This can be explained reasonable: in following wave condition, the slamming forces on the stern are quite considerable because the shape of stern is boxy. However, there is an exception for heading angle of 60° and 120°. Inversely, the C_{fx} of 60° is about 2.3 , four times bigger than that for 120°, making it as the maximal value among all heading angles. This is due to the geometry characteristic of bow. In the case of 60°, the incident angle of wave closes to normal to the bow. This will be discussed in the later section. In oblique wave condition, almost all the CFD results of C_{fx} are less than the EFD results except for 120°. For instance, the CFD result for the heading angle of 30° only covers 78% of EFD result. The cause of these flat CFD results are the wave decay due to the insufficient mesh number along the wavelength. According to ITTC guideline for ship CFD application (2011). For wave simulation, use no less than 20 grid points in the vertical direction and no less than 80 grid points per wavelength on the free surface. In this study, only 50 grid points per wavelength is satisfied. The wavelength in this study is relatively small ($\lambda/L_{pp} = 0.356$) and it will cost a large number of computational source to achieve the recommended mesh number. For the following wave, it can be see that the C_{fx} is overestimated by CFD, which may due to the strong nonlinear behavior of stern wave pattern. The following wave directly impacts on the stern and rudder increasing complexity of the simulation.

The calculated wave drift forces C_{fy} and its measured values are show in Fig. 6 (b). The comparisons show quite well agreement between CFD and EFD. At the heading angle of 90°, its value increases to the peak. Same as the C_{fx} ,these coefficients are under predicted by the CFD, especially for the angle of 90° which is under predicted by 14.13%. The errors of CFD predictions of C_{fy} for other wave angles are in the range 2.7%-10.68%. In the condition of beam wave, the gaps between CFD and EFD may be caused by the simplification of keels. In addition, there is extremely violent wave slamming on the port side which increase the difficulty of simulation.

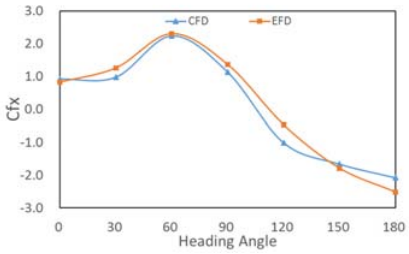

(a) Normalized longitudinal drift forces as function of wave angles

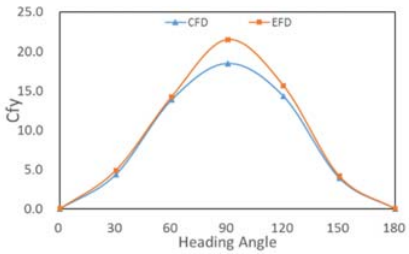

(b) Normalized lateral drift forces as function of wave angles

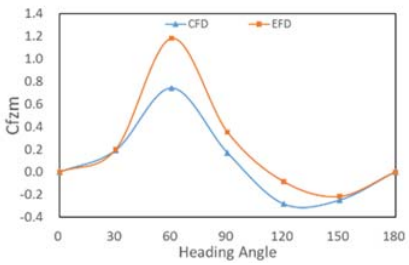

(c) Normalized yaw drift moments as function of wave angles

Fig. 6 Comparison between experimental data and CFD results.

The calculated yaw drift forces C_{fzm} is show in Fig. 6 (c) compared with the EFD results. The comparisons show quite well agreement between CFD and EFD for the angles of 30 and 150. For the 60° and 120°, the results show that there is peak value of yaw moment at the 60°. The reason is that there is strong wave force normally impact on the bow and the distance from a reference point of moments is quite considerable. Similar to the C_{fx}, the yaw moment for 60° is under predicted while that for 120° is overestimated.

Time History of Forces and Moments

The time history of forces and moments for all cases can be found at appendix from Fig.13 to Fig 15. Typically, Fig. 7 compares the time history of forces and moments for 60° and 120°. In Fig. 7(a), the negative value of longitudinal force of 120° is compared with the 60°. Through this way, the positive direction of longitudinal force can be in consistence with the wave incident direction. Figures show that both of their amplitudes of longitudinal and lateral forces are in the same level. However, for the yaw moments, 60° case ,it has extremely large amplitude which is in accordance with the EFD. The nonlinear behavior of these curves of 60° is more notable than 120°.

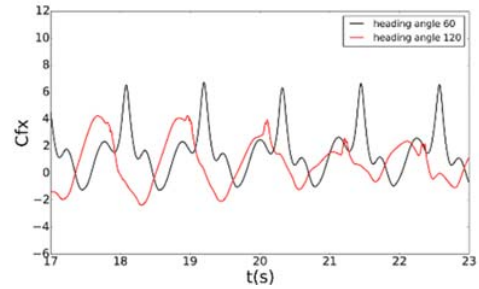

(a) Time history of C_{fx}

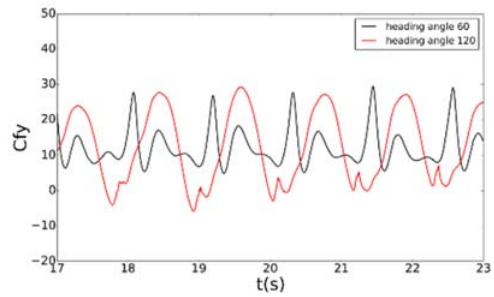

(b) Time history of C_{fy}

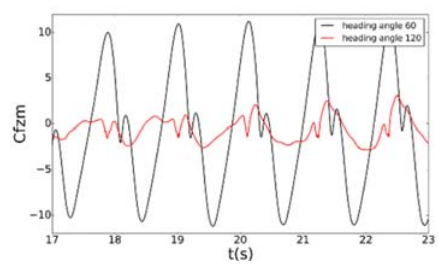

(c) Time history of C_{fzm}

Fig. 7 Time history of longitudinal, lateral forces and yaw moments

In order to analyze the linear and nonlinear effects on forces, the unsteady history of C_{fx} C_{fy} are analyzed by fast Fourier transform (FFT). Fig. 8 indicates that the peak frequency observed at $f_e = 0.886$ is equal to the incidence frequency of the wave. For the case of 120°, there is only solitary peak in the frequency domain. On the contrary, four extreme values can be observed in the FFT result of case 60°.Fig 8 indicates that there are two frequency components comparative to each other for the case of 60°. One of them is the wave frequency and the other one is around 3 s^{-1}. According to the experimental benchmark of DTC (Moctar et al. 2012), the natural frequency of the roll decay motion is around 3 s^{-1} indicating that the roll motions of the hull have a significant effect on the lateral wave force. Besides the two primary peak, there are other two peak frequency components at 1.85 s^{-1} and 3.3 s^{-1}, respectively. Due to the absence of experimental data of natural frequencies for pitch and heave, connections between these two peaks and motions are uncertain. Though it is reasonable to deduce that the pitch and heave induce the other two frequency of forces.

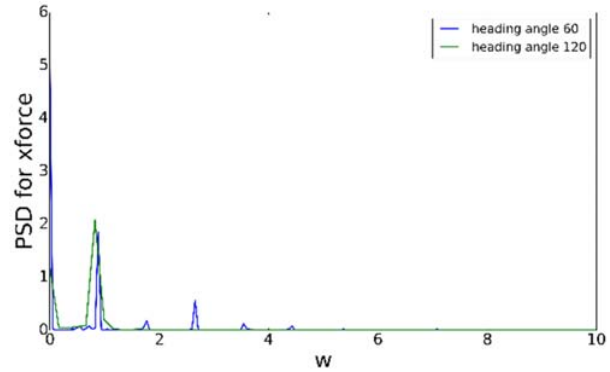

(a) *X* direction force

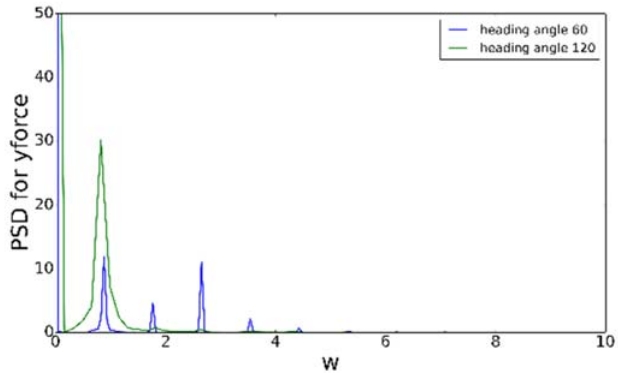

(b) *Y* direction force

Fig. 8 FFT results for longitude forces (a) and lateral forces (b)

Ship Motions

The time history of pitch, roll and heave for all cases can be found at appendix from Fig.16 to Fig.18. All these curves fluctuating within the frequency of waves and the FFT results show that only the wave frequency dominates these motions. The amplitude of pitch motions increases as heading angle changing from 0° to 60° and the same trend is presented when angle changes from 180° to 120°. In the condition of beam wave, the amplitude of pitch motion decrease to a minimum. Fig. 17 illustrates that the roll motions increase while the wave incidence angles became normal to the port side. In the case of 120°, the amplitude of pitch motion increase to a maximum. Fig. 18 shows that beam wave invokes the maximum response of heave motion.

Wave Pattern and Dynamic Pressure

Fig. 9 and Fig. 10 show four snapshots of wave pattern and dynamic pressure with wave condition of 60° and 120°.For these two case, three wave peaks or troughs form at portside while the waves are obstructed at starboard. For the case of 60°, it is obvious that a wave crest directly impacts on the bow at the moment of 21.4 s corresponding to the peak value of C_{fx} and C_{fmz} illustrated in Fig. 7. At t = 21.9 s, A trough can be observed at the bow ,which causes the minimum value of C_{fx}.

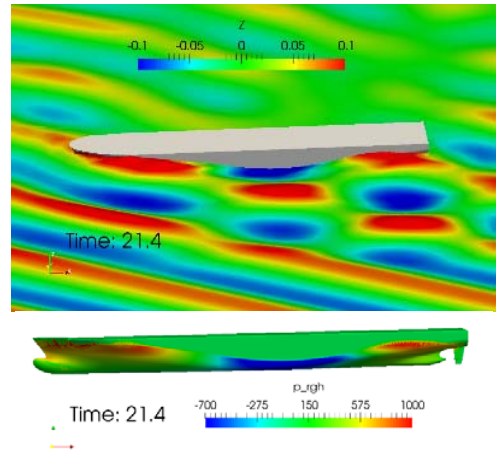

(a) wave patterns and dynamic pressure at t = 21.4 s

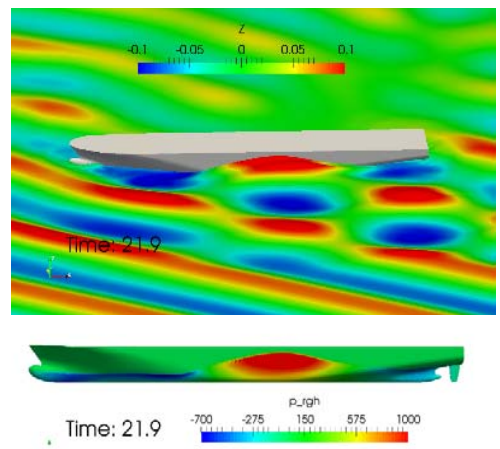

(b) wave patterns and dynamic pressure at t = 21.9 s

Fig. 9 Two snapshots of wave patterns and dynamic pressures in condition of 60° heading angle.

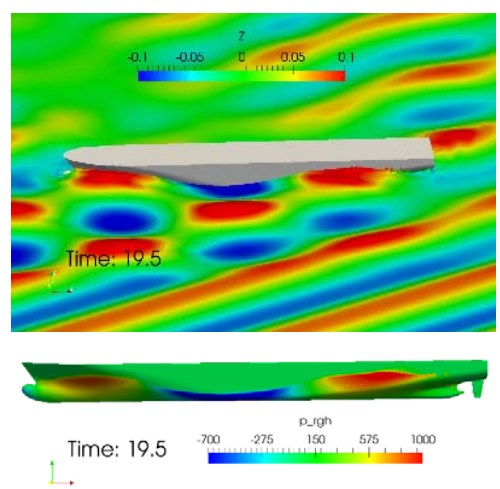

(a) wave patterns and dynamic pressure at t = 19.5 s

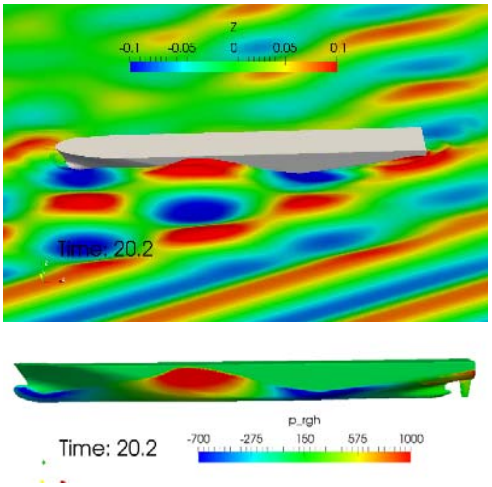

(b) wave patterns and dynamic pressure at t = 20.2 s

Fig. 10 Two snapshots of wave patterns and dynamic pressures in condition of 120° heading angle

Fig. 11 shows two snapshots of wave pattern and dynamic pressure with wave condition of 90°. For this case, one wave peak or trough alternates at portside. At t = 28.1 s, a wave crest directly impacts on the port and the wave crest approach to the deck corresponding to the peak value of C_{fx}. At t = 26.2 s, A trough can be observed at port, which causes the minimum value of C_{fy}. At this moment, the wave trough reaches to the region where there should be keels. As a consequence, the simplification of keels may induce errors in CFD results.

Fig. 12 shows two snapshots of wave pattern with wave condition of 180°. Strong nonlinear phenomenon occurs along with wave peak or trough alternating at stern. At t = 23.8 s, a wave trough arrives at rudder accounting for the rudder surfacing. At t = 23.3 s, a wave crest approach to the deck and directly impacts on the transom plate corresponding to the peak value of C_{fx}. The waves slam on the bottom of stern periodically in this process, which increase the complexity of simulation and raise computational error. As a consequence, there is 17.8% error for the result of C_{fx} of 180°.

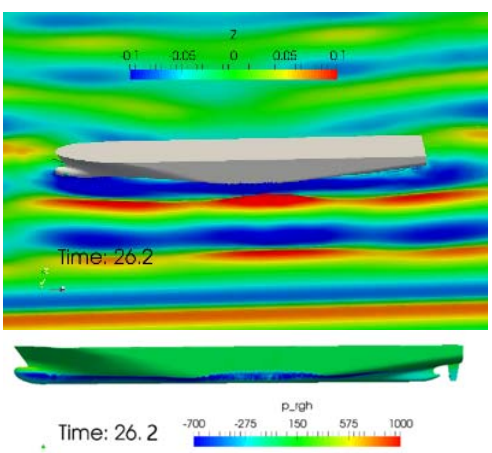

(a) wave patterns and dynamic pressure at t = 26.2 s

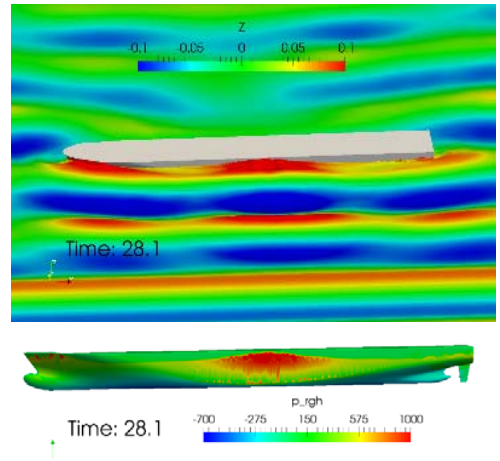

(b) wave patterns and dynamic pressure at t = 28.1 s

Fig. 11 Two snapshots of wave patterns and dynamic pressures in condition of beam wave.

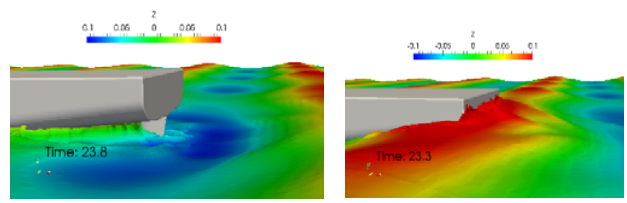

Fig. 12 Two snapshots of wave patterns in condition of following wave.

CONCLUSIONS

In this paper, drift forces and moments are predicted in regular oblique waves, which are performed by our solver, naoe-FOAM-SJTU, developed under the framework of the open source OpenFOAM packages. An open source library waves2Foam is imposed in our solver to handle the wave problem. A post-Panamax 14000 TEU containership, Duisburg Test Case (DTC), is considered in seven wave heading angles without current. The prediction of wave drift forces agrees with the measurements well. The maximum value of longitude drift forces is captured at the heading angle of 60° in our computations. This is due to the incident angle of wave closes to normal to the bow. Another consequence of this strong impact is that the maximum value of wave drift yaw moments also presents at this heading angle. For the C_{fy}, the peak value is obtained by our simulations in the case of 90°, which is in accordance with the EFD. But this value is underestimated caused by two reasons: In the condition of 90°, the wave trough reaches to the keel region so that the simplification of keels may incur error; In addition, Strong nonlinear phenomenon occurs when the wave crest directly impacts on the port side. It causes broken waves which increase the complexities and arise errors. The time history curves of drift forces illustrate that nonlinear behavior is more notable when the wave incident from the bow. The FFT results of drift forces explain that the natural frequency of roll plays a significant role in these time history curves. The time history curves of motions also gain in these simulation. All these curves fluctuating within the frequency of waves and the FFT results show that only the wave frequency dominates these motions.

From the computational results, we can conclude that the presented

solver, naoe-Foam-SJTU, is able to handle the problems about the prediction for the wave drift forces, especially for fully nonlinear problems, such as strong wave impacts on the rudder or stern. This is a fundamental ability to tackle with the maneuverability in waves in the future works.

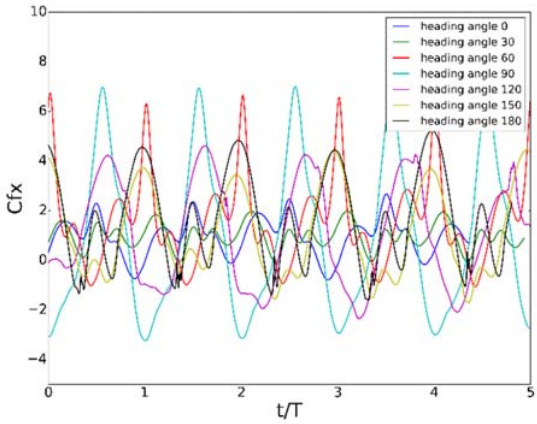

Fig. 13 Time history of longitude forces coefficients

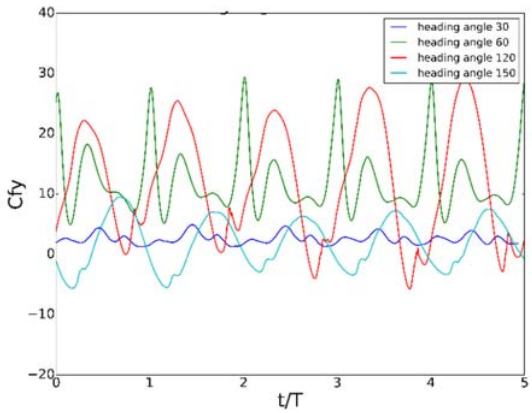

Fig. 14 Time history of lateral forces coefficients

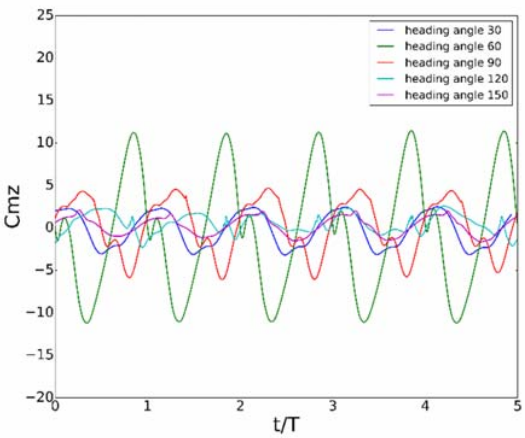

Fig. 15 Time history of yaw moments coefficients

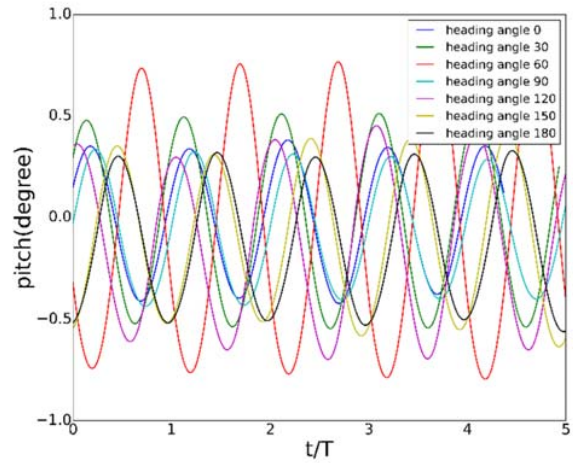

Fig. 16 Time history of pitch motions

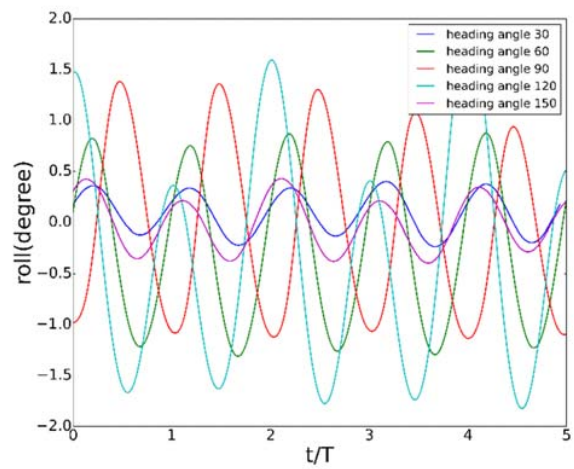

Fig. 17 Time history of roll motions.

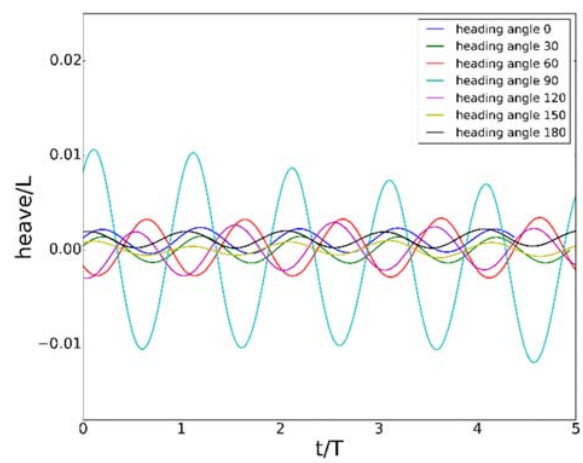

Fig. 18 Time history of heave motions.

ACKNOWLEDGEMENTS

This work is supported by the National Natural Science Foundation of China (51379125, 51490675, 11432009, 51579145), Chang Jiang Scholars Program (T2014099), Shanghai Excellent Academic Leaders Program (17XD1402300), Shanghai Key Laboratory of Marine Engineering (K2015-11), Program for Professor of Special Appointment (Eastern Scholar) at Shanghai Institutions of Higher Learning (2013022), Innovative Special Project of Numerical Tank of Ministry of Industry and Information Technology of China(2016-23/09) and Lloyd's Register Foundation for doctoral student, to which the authors are most grateful.

REFERENCES

Berberović, E, van Hinsberg NP, Jakirlić, S, Roisman, IV, and Tropea, C (2009). "Drop impact onto a liquid layer of finite thickness: dynamics of the cavity evolution." *Phys Rev E*, Vol. 79, No. 3, 36306.

Cao, HJ, Wan, DC, and Yang, C (2013). "Numerical Simulation of Violent Flow of 3-D Dam-Breaking Wave Around Square Cylinder," *Chin J Hydrodyn*, Vol. 28, No. 4, pp.414-422.

Grue, J and Palm, E (1993). "The mean drift force and yaw moment on marine structures in waves and current," *J Fluid Mech*, Vol. 250, pp. 121-142

Hermans, AJ (1999). "Low-frequency second-order wave-drift forces and damping," *J Eng Math*, Vol.35, pp.181-198

ITTC Specialist Committee on CFD in Marine Hydrodynamics (2011). "Practical Guidelines for Ship CFD Application," *26th ITTC*

Jacobsen, NG, Fuhrman, DR, and Fredsøe, J (2012). "A wave generation toolbox for the open-source CFD library: OpenFoam," *Int. J. Numer. Methods Fluids*, Vol. 70, No. 9, pp.1073-1088.

Moctar, O, Sprenger, F, Schellin TE, and Papanikolaou, A (2016). "Numerical and experimental investigations of ship maneuvers in waves", *Proc 35th Int Conf Ocean, Offshore Arctic Eng*, OMAE, Busan, South Korea, OMAE2016-54847

Noack, RW, Boger, DA, Kunz, RF, and Carrica, PM (2009). "Suggar++: an improved general overset grid assembly capability. *Proc 19th AIAA Comp Fluid Dyn Conf*, San Antonio, USA

Orihara H, and Miyata H (2003). "Evaluation of added resistance in regular incident waves by computational fluid dynamics motion simulation using an overlapping grid system", *J Mar Sci Technol*, Vol. 8, pp.47-60

Potthoff, R and Moctar, B (2016). "Presentation of Benchmark results SHOPERA Benchmark Workshop", SHOPERA, London

Rusche, H (2002). "Computational Fluid Dynamics of Dispersed Two-phase Flows at High Phase Fractions," Ph.D. thesis, Imperial College, London, UK,

Sadat-Hosseini, H, Wu, P, Carrica, PM, Kim H, Toda Y, and Stern F (2013). "CFD verification and validation of added resistance and motions of KVLCC2 with fixed and free surge in short and long head waves," *Ocean Eng*, Vol. 59, pp.240–273

Shen ZR and Wan, DC (2013). "RANS Computations of Added Resistance and Motions of a Ship in Head Waves", *Proc 17th Int Offshore and Polar Eng Conf*, Vladivostok, Russia, ISOPE, Vol. 23, pp. 263-271

Shen, ZR, and Wan, DC (2011). "Numerical Simulation of Sphere Water Entry Problem Based on VOF and Dynamic Mesh Methods," *Proc 21st Int Offshore Polar Eng Conf*, Maui, Hawaii, USA, ISOPE, Vol.3, pp.695-702.

Shen, ZR, and Wan, DC (2012). "Numerical Simulations of Large-Amplitude Motions of KVLCC2 with Tank Liquid Sloshing in Waves," *Proc 2nd Int Conf Violent Flows*, Nantes, France, Ecole Centrale Nantes, pp.149-156.

Shen, ZR, Wan, DC and Carrica, PM (2015). "Dynamic overset grids in OpenFOAM with application to KCS self-propulsion and maneuvering." *Ocean Eng*, Vol.108, pp.287-306.

Sprenger, F, Hassani, V, Maron, A (2016). "Establishment of a validation and benchmark database for the assessment of ship operation in adverse conditions," *Proc 35th Int Conf Ocean, Offshore Arctic Eng*, Busan, South Korea, OMAE2016-54865

Tanizawa, K, Minami M, and Sawada, H (2000). "Estimation of Wave Drift Force by Numerical Wave Tank: 2nd Report," *Proc 10th Int Offshore Polar Eng Conf*, Seattle, USA, ISOPE, Vol. 3, pp.237-244

Wang, JH, Zhao, WW, Wan, DC (2016 a). "Self-propulsion Simulation of ONR Tumblehome Using Dynamic Overset Grid Method," *Proc 7th Int Conf Comput Method*, Berkeley, USA, ICCM, No. ID 1499-5539-1-PB.

Wang, JH, Zhao, WW and Wan, DC (2016 b). "Free Maneuvering Simulation of ONR Tumblehome Using Overset Grid Method in naoe-FOAM-SJTU", *Proc 31st Symp Naval Hydrodyn*, California, USA, Paper No. 16

Yang, K and Kim, Y (2015). "Cartesian-grid-based computational analysis for added resistance in waves", *J Mar Sci Technol*, Vol. 20, pp.155-170